JCTC Journal of Chemical Theory and Computation

Antisymmetric Magnetic Interactions in Oxo-Bridged Copper(II) Bimetallic Systems

R. Maurice,[†,‡] A. M. Pradipto,[§] N. Guihéry,*[,†] R. Broer,[§] and C. de Graaf*[,||,‡]

Laboratoire de Chimie et Physique Quantiques, Université de Toulouse 3, 118, route de Narbonne, 31062 Toulouse France, Departament de Química Física i Inorgànica, Universitat Rovira i Virgili, Marcel·lí Domingo s/n, 43007 Tarragona, Spain, Zernike Institute for Advanced Materials, University of Groningen, Groningen 9747AG, The Netherlands, and Institució Catalana de Recerca i Estudis Avançats (ICREA), Passeig Lluis Companys 23, 08010, Barcelona, Spain

Received June 15, 2010

Abstract: The antisymmetric magnetic interaction is studied using correlated wave-function-based calculations in oxo-bridged copper bimetallic complexes. All of the anisotropic multispin Hamiltonian parameters are extracted using spin−orbit state interaction and effective Hamiltonian theory. It is shown that the methodology is accurate enough to calculate the antisymmetric terms, while the small symmetric anisotropic interactions require more sophisticated calculations. The origin of the antisymmetric anisotropy is analyzed, and the effect of geometrical deformations is addressed.

1. Introduction

The combined effect of spin−orbit coupling (SOC) and spin−spin coupling (SSC) can lead to magnetic anisotropy without the necessity of applying an external magnetic field. In addition to the presence of unpaired electrons, the system should be not too symmetric to present measurable magnetic anisotropy effects and to avoid the presence of unquenched orbital momentum.[1,2] This effect has been encountered in organic molecules,[3] monometallic transition metal complexes,[4,5] single-molecule magnets (SMMs),[6] and extended materials related to the cuprate high-T_c superconductors.[7,8] Antisymmetric interactions were introduced phenomenologically in 1958 by Dzyaloshinskii[9] to describe the magnetic properties of α-Fe_2O_3. The theory was generalized by Moriya two years later,[10] leading to the well-known standard multispin Hamiltonian for binuclear systems with $S = 1/2$ magnetic centers:[2,4]

$$\hat{H} = J\hat{\mathbf{S}}_a \cdot \hat{\mathbf{S}}_b + \hat{\mathbf{S}}_a\bar{\bar{D}}\hat{\mathbf{S}}_b + \vec{d}\hat{\mathbf{S}}_a \times \hat{\mathbf{S}}_b \quad (1)$$

This model involves an isotropic exchange term J, a symmetric zero field splitting (ZFS) tensor $\bar{\bar{D}}$, and the antisymmetric part that is described by the Dzyaloshinskii−Moriya (DM) pseudovector $\vec{d}$. Interpretation of experimental data led to detailed information about spin canting in copper oxides and explained the origin of the weak ferromagnetism in some of the crystallographic phases despite the strong antiferromagnetic isotropic exchange. Recently, the norm of the DM vector was determined in $SrCu_2(BO_3)_2$ through electron paramagnetic resonance (EPR) spectroscopy.[11,12] On the basis of the perturbational approach outlined by Moriya, there have been many attempts to rationalize the anisotropic interaction between two Cu^{2+} ions.[13−16] A systematic overview has recently been published by Moskvin.[17]

Until now, the *ab initio* study of magnetic anisotropy has been mainly limited to the monometallic complexes or the symmetric terms in polynuclear systems. One of the first anisotropy calculations was performed on a titanium bimetallic complex, combining the complete active space self-consistent field (CASSCF) approach, multireference perturbation theory (MRPT), and effective nuclear charge SOC calculations.[18] The implementation of SOC in the NRLMOL code[19,20] triggered a major breakthrough in the application of density functional theory (DFT) to the magnetic anisotropy

* Corresponding author e-mail: nathalie.guihery@irsamc.ups-tlse.fr (N.G.); coen.degraaf@urv.cat (C.d.G.).
[†] Université de Toulouse 3.
[‡] Universitat Rovira i Virgili.
[§] University of Groningen.
[||] ICREA.

10.1021/ct100329n © 2010 American Chemical Society
Published on Web 09/24/2010

in polymetallic SMMs.[21−27] An *ab initio* treatment of SSC was presented by Vahtras et al.[28] Another important contribution was made by Neese with the implementation of SOC and SSC in the ORCA code.[29] This implementation not only allows the study of anisotropy with DFT but also paved the way for the use of wave-function-based methodologies.[30−32] The latter methods have been applied successfully to several monometallic transition metal complexes and organic systems.[33−38] A similar treatment of SOC was implemented in the MOLCAS code[39] based on the restricted active space state interaction spin−orbit (RASSI-SO) scheme,[40,41] which was used to study ZFS phenomena in transition metal complexes.[42−49] Finally, we mention the work of Gilka et al. on SSC[50] and the ZFS calculations on organic molecules by Sugisaki and co-workers.[51]

The binuclear copper(II) acetate complex described by Bleaney and Bowers[52] is one of the first examples of a polynuclear system with anisotropic interactions and has been the subject of several studies.[53−55] Since this complex presents a center of inversion, only symmetric interactions are allowed, and we will treat the anisotropy of this system in a separate study. Antisymmetric interactions in binuclear complexes are less common and difficult to probe by EPR spectroscopy.[56] Some synthetic complexes were proposed by Kahn to present antisymmetric interactions,[57] but the only clear evidence of DM interaction in a bimetallic complex was found in a diferric complex and has required the use of Mössbauer spectroscopy.[58] Important antisymmetric interactions have also been evidenced in trimetallic copper(II) complexes by both magnetic circular dichroism (MCD) and EPR spectroscopies.[59]

Recently, a new extraction method of anisotropic parameters has been proposed[47] that is based on effective Hamiltonian theory.[60,61] The method establishes a simple procedure to determine the ZFS parameters and the magnetic anisotropic axes. In addition, the method can be used to validate existing model Hamiltonians to describe the magnetic anisotropy. The standard multispin Hamiltonian for centrosymmetric bimetallic systems was found to be incomplete, lacking a non-negligible biquadratic anisotropic interaction term.[48]

To add a new aspect to the understanding of the anisotropic interactions between two Cu(II) ions bridged by a diamagnetic bridge, we apply the new extraction method to a Cu(II) model complex that mimics the Cu−O−Cu units present in copper oxides and that is also relevant to molecular polynuclear Cu(II) complexes. The application of *ab initio* calculations and subsequent mapping on a model Hamiltonian through effective Hamiltonian theory allows us to extract all parameters of the general spin Hamiltonian written in eq 1 and to investigate the mechanism of anisotropy without any assumption. For example, we do not assume that the anisotropy solely arises from the interaction of the fundamental singlet and triplet with excited states. In addition, we determine the relative importance of all of the terms that were described by Moskvin by means of a decomposition of the *ab initio* wave function and study the effect on the anisotropy of the bending of the central Cu−O−Cu bond ϑ_1 and the twisting of the two CuO_4 planes defined as the dihedral angle ϑ_2 shown in Figure 1.

2. Theory and Methodology

2.1. Spin Hamiltonian in Copper(II) Bimetallic Systems.

We start our analysis with the derivation of the 4 × 4 interaction matrix spanned by the singlet and triplet $|S,M_S\rangle$ determinants. For convenience, we rewrite eq 1 by grouping the symmetric and antisymmetric anisotropic interaction in a single second-order tensor T:

$$\hat{H} = J\hat{\mathbf{S}}_a \cdot \hat{\mathbf{S}}_b + \hat{\mathbf{S}}_a \bar{\bar{T}} \hat{\mathbf{S}}_b \tag{2}$$

The easiest way to proceed is to build the model interaction matrix in the uncoupled $|M_{S_a},M_{S_b}\rangle$ basis taking into account all possible interactions in an arbitrary axis frame. M_{S_a} and M_{S_b} are the M_S components of the local doublets on centers a and b, respectively.

$\hat{H}_{\mathrm{mod}}$	$\left\|-\frac{1}{2},-\frac{1}{2}\right\rangle$	$\left\|-\frac{1}{2},\frac{1}{2}\right\rangle$	$\left\|\frac{1}{2},-\frac{1}{2}\right\rangle$	$\left\|\frac{1}{2},\frac{1}{2}\right\rangle$
$\left\langle-\frac{1}{2},-\frac{1}{2}\right\|$	$\frac{1}{4}(J+T_{33})$	$-\frac{1}{4}(T_{31}+iT_{32})$	$-\frac{1}{4}(T_{13}+iT_{23})$	$\frac{1}{4}[T_{11}-T_{22}+i(T_{12}+T_{21})]$
$\left\langle-\frac{1}{2},\frac{1}{2}\right\|$	$-\frac{1}{4}(T_{31}-iT_{32})$	$-\frac{1}{4}(J+T_{33})$	$\frac{1}{2}J+\frac{1}{4}[T_{11}+T_{22}+i(T_{21}-T_{12})]$	$\frac{1}{4}(T_{13}+iT_{23})$
$\left\langle\frac{1}{2},-\frac{1}{2}\right\|$	$-\frac{1}{4}(T_{13}-iT_{23})$	$\frac{1}{2}J+\frac{1}{4}[T_{11}+T_{22}-i(T_{21}-T_{12})]$	$-\frac{1}{4}(J+T_{33})$	$\frac{1}{4}(T_{31}+iT_{32})$
$\left\langle\frac{1}{2},\frac{1}{2}\right\|$	$\frac{1}{4}[T_{11}-T_{22}-i(T_{12}+T_{21})]$	$\frac{1}{4}(T_{13}-iT_{23})$	$\frac{1}{4}(T_{31}-iT_{32})$	$\frac{1}{4}(J+T_{33})$

In a second step, the model matrix is transformed to the coupled $|S,M_S\rangle$ basis for a more straightforward understanding of the interactions:

$\hat{H}_{\mathrm{mod}}$	$\lvert 1,-1\rangle$	$\lvert 1,0\rangle$	$\lvert 1,1\rangle$	$\lvert 0,0\rangle$
$\langle 1,-1\rvert$	$\frac{1}{4}(J+T_{33})$	$-\frac{\sqrt{2}}{8}[T_{13}+T_{31}+i(T_{23}+T_{32})]$	$\frac{1}{4}[T_{11}-T_{22}+i(T_{12}+T_{21})]$	$-\frac{\sqrt{2}}{8}[T_{13}-T_{31}+i(T_{23}-T_{32})]$
$\langle 1,0\rvert$	$-\frac{\sqrt{2}}{8}[T_{13}+T_{31}-i(T_{23}+T_{32})]$	$\frac{1}{4}(J+T_{11}+T_{22}-T_{33})$	$\frac{\sqrt{2}}{8}[T_{13}+T_{31}+i(T_{23}+T_{32})]$	$-\frac{i}{4}(T_{12}-T_{21})$
$\langle 1,1\rvert$	$\frac{1}{4}[T_{11}-T_{22}-i(T_{12}+T_{21})]$	$\frac{\sqrt{2}}{8}[T_{13}+T_{31}-i(T_{23}+T_{32})]$	$\frac{1}{4}(J+T_{33})$	$-\frac{\sqrt{2}}{8}[T_{13}-T_{31}-i(T_{23}-T_{32})]$
$\langle 0,0\rvert$	$-\frac{\sqrt{2}}{8}[T_{13}-T_{31}-i(T_{23}-T_{32})]$	$\frac{i}{4}(T_{12}-T_{21})$	$-\frac{\sqrt{2}}{8}[T_{13}-T_{31}+i(T_{23}-T_{32})]$	$\frac{1}{4}(-3J-T_{11}-T_{22}-T_{33})$

The symmetric and antisymmetric contributions (D_{ij} and d_{ij}, respectively) can be separated as follows:

$$\begin{aligned} D_{ii} &= T_{ii} \\ D_{ij} &= D_{ji} = \frac{1}{2}(T_{ij}+T_{ji}) \\ d_{ij} &= -d_{ji} = \frac{1}{2}(T_{ij}-T_{ji}) \end{aligned} \tag{3}$$

From this, it is clear that the antisymmetric interactions arise from the $\langle S,M_S|H_{\mathrm{mod}}|S',M_S'\rangle$ matrix elements and cause a direct coupling between the singlet and triplet states, which is absent in the case of symmetric interactions only. Finally, we mention that the antisymmetric second order tensor $\bar{\bar{d}}$ can be reduced to a pseudovector with the following components:

$$d_x = d_{23} \quad d_y = -d_{13} \quad d_z = d_{12} \tag{4}$$

2.2. Description of the Models and Computational Information. The model complex used in the calculations consists of a Cu−O−Cu central part using H_2O ligands to complete the coordination sphere of the copper ions. The Cu−O distances have been fixed to 2.00 Å and the O−H distances fixed to 0.96 Å, while the ϑ_1 and ϑ_2 angles are susceptible to changes. The symmetry rules for the appearance of both symmetric and antisymmetric interactions are well-known and reported in the literature.[62] In the case where $\vartheta_1 = \vartheta_2 = 0°$, the complex has an inversion center, and hence, only symmetric anisotropic interactions are allowed. When ϑ_1 is changed, the symmetry is lowered from D_{2h} to C_{2v} and a DM vector appears along the z axis. The twist of the CuO_4 planes ($\vartheta_2 \neq 0°$) lowers the symmetry to D_2 and induces a DM vector aligned along the x axis. However, the interaction is strictly zero when the planes are orthogonal ($\vartheta_1 = 0°$, $\vartheta_2 = 90°$) and the molecule has D_{2d} symmetry. When both distortions are present, the point group symmetry is C_2 with just a 2-fold rotation axis along the y axis. In this case, the DM vector lies in the xz plane.

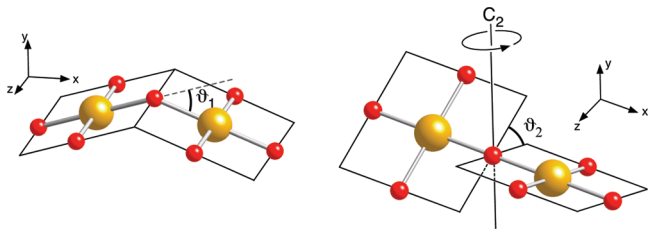

Figure 1. Schematic representation of the distortions applied to the model complex. Large spheres represent copper, and smaller spheres are oxygens.

The SSC is an important mechanism to describe anisotropy when the ZFS is on the order of a few cm^{-1}. However, it does not lead to antisymmetric interactions, as it cannot directly couple triplet with singlet states.[63] As our main objective of this study concerns the description of the DM interaction, that is, the effective coupling between singlet and triplet states, only the SOC has been considered. We follow a two-step procedure implemented in Molcas 7 to obtain accurate estimates of the exact N-electron wave function that account for dynamic electron correlation and spin−orbit interactions.

First, a number of spin−orbit free states is computed via the CASSCF method using the Douglas−Kroll−Hess Hamiltonian.[64,65] The active space contains all Cu-3d orbitals and the corresponding 18 electrons. CASSCF wave functions can be defined for all 25 singlet and triplet states of the d^9−d^9 manifold excluding the metal-to-metal charge transfer states. Second, the spin−orbit coupling is introduced *a posteriori* via the RASSI-SO method.[40,41] This method uses the mean-field approximation and the one-center approximation,[66] through the so-called atomic-mean field integrals (AMFI).[67,68] Dynamic correlation effects can be introduced by replacing the diagonal elements of the spin−orbit matrix by CASPT2 energies[69,70] using the CAS(18,10)SCF wave function as a reference. Following the conclusions of a previous work on the magnetic coupling,[71] the IPEA shift of the CASTP2 zeroth-order Hamiltonian is set to zero.[72,73] An imaginary level shift of 0.2 hartree was applied to avoid the appearance of intruder states in the perturbational treatment of dynamical electron correlation.[74] The following ANO-RCC basis set[75] was used: Cu (6s 5p 4d 2f), O (4s 3p 1d), and H (2s).

In addition to the large CAS(18,10), we also performed calculations with a minimal CAS(2,2) containing the magnetic orbitals only, in which we can just define the ground state singlet and triplet states.

2.3. Extraction of Spin Hamiltonian Parameters. The interaction matrix presented in section 2.1 contains 10 parameters. This number is reduced to seven when the molecule is oriented is such a way that the magnetic axes frame coincides with the Cartesian axes frame. Since the model space is spanned by the four $|M_S\rangle$ components of the singlet and triplet, it is not possible to determine all the parameters from the energy differences only. For the same reason, it is also complicated to extract both symmetric and antisymmetric interactions in the general case from an experiment, for instance from EPR spectra.[56] The required extra information is contained in the wave function of the spin−orbit states and is used to construct an effective Hamiltonian[60] that allows us to extract all 10 parameters.

The effective Hamiltonian is determined by projecting the states that span the SO−SI space onto the model space. The projections with the largest norm are orthonormalized by the procedure of des Cloizeaux,[61] and the matrix elements of the effective Hamiltonian are calculated by applying the following formula:

$$\langle \Phi_i | \hat{H}^{\text{eff}} | \Phi_j \rangle = \langle \Phi_i | \sum_{k=1}^{4} | \tilde{\Psi}_k \rangle E_k \langle \tilde{\Psi}_i | \Phi_j \rangle \tag{5}$$

where $\Phi_{i,j}$ are the four M_S components arising from the singlet and triplet spanning the model space, $\tilde{\Psi}_k$ represents the orthonormalized projections of the *ab initio* wave functions, and E_k represents the corresponding energies. A more comprehensive description of the application of the effective Hamiltonian theory to extract anisotropy parameters can be found in refs 47 and 48. The comparison of these numerical matrix elements with those of the model Hamiltonian of section 2.1 leads to nine independent equations. The axial and rhombic anisotropy parameters D and E are usually defined in the magnetic axes frame as

$$\begin{aligned} D &= D_{zz} - \frac{1}{2}(D_{xx} + D_{yy}) = \frac{3}{2}D_{zz} \\ E &= \frac{1}{2}(D_{xx} - D_{yy}) \end{aligned} \tag{6}$$

The magnetic axes frame is obtained by diagonalizing the symmetric ZFS tensor and by applying the standard conventions of molecular magnetism that $|D| > 3E > 0$. While the first convention ($|D| > 3E$) fixes the attribution of the z magnetic axis as the hard or easy axis of magnetization, the second one fixes the attribution of the magnetic axes x and y by imposing E to be positive. Then, the magnetic axes frame is univocally defined.

The one-by-one comparison of the model and effective Hamiltonian establishes a way to determine the ability of the model Hamiltonian to describe the electronic interactions of the exact Hamiltonian used to obtain the *ab initio* results. This strategy revealed the existence of higher-order anisotropic interactions in bimetallic complexes with $S \geq 1$ magnetic centers.[48] Since these interactions cannot occur for the Cu(II) dimer under study, the only possible source of discrepancy between the effective and model Hamiltonian is the presence of orbital degeneracy. The model Hamiltonian should imply both spin and orbital degrees of freedom in the latter case.[76] However, the coordination of the Cu(II) ions leads to a nondegenerate ground state, and it is expected that the standard multispin Hamiltonian of eq 1 accurately accounts for the anisotropy.

3. Results and Discussion

3.1. Validation of the Spin Hamiltonian. To address the validity of the standard spin Hamiltonian and to illustrate the extraction procedure, one example will be presented in certain detail. The numbers listed in this section are calculated for the structure with $\vartheta_1 = \vartheta_2 = 45°$, but the conclusions are also valid for the other structures discussed afterward. All numbers presented in the text and equations of this paragraph are given in cm^{-1} unless specified otherwise. The RASSI-SO calculation is performed with a SI space of 25 triplet and 25 singlet spin-free states. The wave function of these states is obtained through a CAS(18/10)SCF calculation. The diagonal matrix elements of the SI matrix correspond to the CASSCF energies of the respective states. The norm of the projection onto the model space of the four low-lying spin−orbit states is approximately 98%. Hence, the model space of the spin Hamiltonian is perfectly adequate in this case. Then, the effective Hamiltonian matrix is calculated applying eq 5:

$\hat{H}_{\text{eff}}$	$\lvert 1,-1\rangle$	$\lvert 1,0\rangle$	$\lvert 1,1\rangle$	$\lvert 0,0\rangle$
$\langle 1,-1\rvert$	50.557	0.024	0.168	$0.657i$
$\langle 1,0\rvert$	0.024	49.781	−0.024	$7.015i$
$\langle 1,1\rvert$	0.168	0.024	50.557	$-0.657i$
$\langle 0,0\rvert$	$-0.657i$	$7.015i$	$0.657i$	1.006

(7)

The term-by-term comparison of this matrix with the model matrix presented in section 2.1 fully validates the model Hamiltonian. The effective Hamiltonian matrix does not show any deviation with respect to the model matrix. Hence, we can proceed to the extraction of the parameters of the model Hamiltonian. The trace of the effective Hamiltonian is arbitrary. As the aim of the model Hamiltonian is to reproduce the relative energies of the low-lying magnetic spectrum, we set the energy of the lowest lying eigenstate of the effective Hamiltonian to zero for convenience. The symmetric ZFS tensor is considered traceless, allowing the extraction of the 10 parameters of the model Hamiltonian. The extracted J value is 49.3 cm^{-1}, and the ZFS tensor is

$$\bar{\bar{T}} = \begin{pmatrix} -0.181 & 14.030 & -0.068 \\ -14.030 & -0.853 & -1.858 \\ -0.068 & 1.858 & 1.034 \end{pmatrix} \tag{8}$$

The symmetric and antisymmetric parts are then separated:

$$\bar{\bar{D}} = \begin{pmatrix} -0.181 & 0 & -0.068 \\ 0 & -0.853 & 0 \\ -0.068 & 0 & 1.034 \end{pmatrix} \tag{9}$$

$$\bar{\bar{d}} = \begin{pmatrix} 0 & 14.030 & 0 \\ -14.030 & 0 & -1.858 \\ 0 & 1.858 & 0 \end{pmatrix} \tag{10}$$

Since the C_2 rotation axis coincides with the Cartesian y axis, D_{12}, D_{23}, and d_{13} are zero.[62] The antisymmetric second-order ZFS tensor can be reduced to a pseudovector $\vec{d} = (-1.858, 0.0, 14.030)$ with a norm of 14.15 cm^{-1}. Since only its orientation and norm can be determined, the DM vector is a so-called pseudovector.

Next, we diagonalize the symmetric ZFS tensor to obtain the magnetic anisotropy axes. Taking care of the usual conventions for the definition of the x, y, and z magnetic anisotropy axes, we obtain $D_{xx} = -0.184$, $D_{yy} = -0.853$, and $D_{zz} = 1.038$.

The magnetic y axis corresponds to the Cartesian y axis (i.e., the C_2 symmetry axis), whereas the magnetic x and z axes nearly coincide with the Cartesian axes. The DM vector can be re-expressed in the magnetic axes frame in order to define its orientation with respect to the anisotropy axes: $\vec{d}$

Table 1. Spin-Free and RASSI-SO J Parameter (cm^{-1}) for Several Model Geometries[a]

	J (spin-free)		J (RASSI-SO)	
$\vartheta_1 = \vartheta_2$	CASSCF	CASPT2	CASSCF	CASPT2
0°	153	562	151	557
15°	138	515	136	509
45°	50	236	49	232
75°	−18	−19	−17	−20
90°	−20	−97	−21	−96

[a] RASSI-SO calculations were performed with 25 triplet and 25 singlet spin-free states. The energies of the spin-free states are calculated with CASSCF and CASPT2 using a CAS(18,10).

= (−1.070, 0.0, 14.120). As expected from symmetry arguments, the DM vector is perpendicular to the C_2 axis, it lies in the xz plane. It makes an angle of −4.3° with the magnetic z axis.

In short, we have shown that the standard multispin Hamiltonian is valid for the Cu(II) dimer and that all ZFS parameters and magnetic axis can be extracted from the *ab initio* calculations in a straightforward manner. It remains to be determined how robust these extracted parameters are against the details of the computational scheme. Ideally, the extracted parameters should not be too sensitive to these degrees of freedom as is the case for the ZFS parameters in the mono- and bimetallic complexes studied before.[47,48]

3.2. Dynamic Correlation Effect on Spin Hamiltonian Parameters. The isotropic magnetic coupling parameter J can be extracted either at the spin-free level or after a RASSI-SO calculation. As the magnetic triplet and singlet states interact differently with the excited states, the RASSI-SO extracted J value can be different from the spin-free extraction. However, as can be seen in Table 1, this effect is nearly negligible. As expected, J is large and antiferromagnetic for the undistorted complex ($\vartheta_1 = \vartheta_2 = 0$) but quickly decreases with the deformations. In fact, the main effect comes from the ϑ_1 deformation angle that induces the change from a large antiferromagnetic coupling (J positive) to a moderate ferromagnetic one (J negative). This result is in agreement with the Goodenough−Kanamori−Anderson rules.[77−79] Dynamic correlation strongly affects the isotropic coupling, as observed in many other studies present in the literature.

The symmetric part of the ZFS tensor is determined by the $\langle 1,M_S|\hat{H}|1,M_S\rangle$ and $\langle 1,M_S|\hat{H}|1,M'_S\rangle$ terms of the effective Hamiltonian, while the antisymmetric part is determined by the $\langle S,M_S|\hat{H}|S',M_S\rangle$ and $\langle S,M_S|\hat{H}|S',M'_S\rangle$ terms. Moreover, the isotropic coupling can be extracted from the difference between the barycenter of the $\langle 1,M_S|\hat{H}|1,M_S\rangle$ type terms and the $\langle 0,0|\hat{H}|0,0\rangle$ term of the effective Hamiltonian. Hence, all different terms (symmetric, antisymmetric, and isotropic) are rigorously separated in the extraction. The extracted symmetric part can then only be affected computationally by changing the magnitude of mechanisms that affects directly the symmetric terms, i.e., by changing the relative energies of the excited spin−orbit free states with respect to the magnetic triplet ground state. Hence, the effect of dynamic correlation on the ZFS parameters D and E passes through the correction of these relatives energies and not through the correction of the J value. Table 2 shows how the dynamic correlation strongly affects D and E. The most obvious manifestation of this effect is the fact that the sign of D is changed using CASPT2 energies in three cases. This change of sign causes a reorientation of the magnetic axis frame in which the roles of the magnetic x and z axes are interchanged.

Table 2. Symmetric Anisotropy Parameters D and E (in cm^{-1}) for Several Model Geometries Extracted from the RASSI-SO Calcualtions with 25 Triplet and 25 Singlet Spin-Free States[a]

	CASSCF		CASPT2	
$\vartheta_1 = \vartheta_2$	D	E	D	E
0°	−0.81	0.04	−0.45	0.01
15°	−1.52	0.02	−0.71	0.14
45°	1.56	0.33	−1.66	0.20
75°	3.38	0.10	−3.27	0.57
90°	4.60	0.27	−4.10	1.22

[a] The use of CAS(18,10)SCF energies for the spin-free states is compared to the use of CASPT2 energies.

It should be noted that the extracted values are small and that the sign of D and the orientation of the magnetic axes frame obtained with the computational approach outlined in the previous section should be benchmarked against calculations at a higher level of theory. Probably, the RASSI-SO matrix elements have to be calculated with wave functions that account for dynamic correlation (i.e., beyond the presently used CASSCF wave functions). Eventually, the CASPT2 spin-free energies should also be replaced by energies obtained with variational techniques as the difference dedicated CI method. Such a study is currently being performed for the copper acetate molecule and will be the subject of another publication.

We will now show that, contrary to the symmetric interactions, the antisymmetric part of the anisotropy tensor is robust against the inclusion of dynamic correlation. The DM interaction can be split into two parts. The first one is the direct coupling between the magnetic triplet and singlet by spin−orbit interaction, the first-order contribution to the DM interaction. Being an off-diagonal element of the model Hamiltonian (see section 2.1), this interaction is hardly affected by the inclusion of dynamic correlation. The second part includes all mechanisms involving excited states, which appear in second-order perturbation theory. The effect of these mechanisms on the DM interaction depends directly on the changes in the excitation energies due to dynamic correlation.

Comparison of the results obtained with CAS(18,10)SCF and CASPT2 listed in Table 3 shows that the dynamic correlation effect influences the norm and the orientation of the DM vector in a modest way. The largest change in the angle is observed for $\vartheta_1 = \vartheta_2 = 75°$, for which φ changes by ∼25°. Although this may indicate a rather drastic change at first sight, the effect is not so large if we compare the d_x and d_z components of the DM vector with and without taking into account the dynamic correlation. Using CASSCF energies, d_z and d_x are −4.8 and 1.4 cm^{-1}, respectively. These values change to −6.7 and −0.8 cm^{-1} when electron correlation is taken into account by CASPT2. Hence, by no means do we observe the drastic changes that occur for the symmetric anisotropy, and we conclude that the effect of

Table 3. Norm of the DM Vector $|\vec{d}|$ (in cm^{-1}) and Angle φ (in deg) of the DM Vector with the Cartesian z Axis for Several Model Geometries[a]

	CAS(2,2)/small RASSI-SO		CAS(18,10)/large RASSI-SO		CASPT2	
$\vartheta_1 = \vartheta_2$	$\|\vec{d}\|$	φ	$\|\vec{d}\|$	φ	$\|\vec{d}\|$	φ
0°	0.00	0.0	0.00	0.0	0.00	0.0
15°	8.35	−0.7	6.98	0.7	9.77	17.2
45°	17.58	−8.5	14.15	−7.5	17.75	7.4
75°	7.78	−17.1	4.97	−16.5	6.76	6.6
90°	7.58	−16.5	7.32	−15.3	6.75	−28.3

[a] The small RASSI-SO space is spanned by the fundamental singlet and triplet states. The large RASSI-SO space contains 25 triplet and 25 singlet spin-free states. The energies of the spin-free states are calculated with CAS(2,2)SCF, CAS(18,10)SCF, and CASPT2.

dynamic correlation is not essential for a semiquantitative description of the DM vector in the Cu−O−Cu system.

To separate the first-order mechanisms involving the singlet and triplet ground states from the second-order mechanisms involving excited states, we performed additional CASSCF/RASSI-SO calculations in which the effect of excited states is completely eliminated. This can be achieved by reducing the active space to two orbitals with two electrons and building the RASSI-SO matrix in the space spanned by the four $|M_S\rangle$ components of the singlet and triplet ground states. Table 3 compares the results obtained with the small RASSI-SO space using the CAS(2,2)SCF wave functions and energies to those obtained with the large CAS and large RASSI-SO space used so far. Again, we observe that the essentials of the DM interaction are maintained. This means that the leading mechanism for antisymmetric anisotropy in Cu−O−Cu-based systems is the direct coupling between the singlet and triplet ground states and that the second-order processes involving excited N-electron states have a smaller effect. In the following, we will apply CAS(2,2)SCF calculations followed by RASSI-SO calculations involving only the singlet and triplet ground states to study in more detail the effect of geometrical deformations and analyze the mechanism of the DM interaction.

3.3. Magneto-Structural Correlations. To complete the study of the geometrical distortion, we calculated the norm of the DM vector as a function of the Cu−O−Cu bending (ϑ_1) and the twist angle of the two CuO_4 planes (ϑ_2). The results are shown in Figure 2. The ϑ_1 deformation leads to the C_{2v} point group symmetry with the DM vector oriented along the Cartesian z axis. As can be seen in Figure 2, this deformation creates a large DM interaction with a maximum of 14.8 cm^{-1} for $\vartheta_1 = 40°$. The DM vector is obviously zero for 0° and 3.6 cm^{-1} for the other extreme when $\vartheta_1 = 90°$.

The start and end points of the twist deformation ($\vartheta_2 = 0°$ and 90°) do not show any DM interaction due to symmetry reasons.[62] In between, there is a small DM vector along the C_2 axis that connects the two magnetic centers. However, according to Figure 2, this deformation on its own does not create any significant antisymmetric anisotropy. The combination of the two deformations leads to an important synergistic effect. The highest norm of the DM vector is 25.5 cm^{-1} and occurs for $\vartheta_1 = 45°$ and $\vartheta_2 = 90°$.

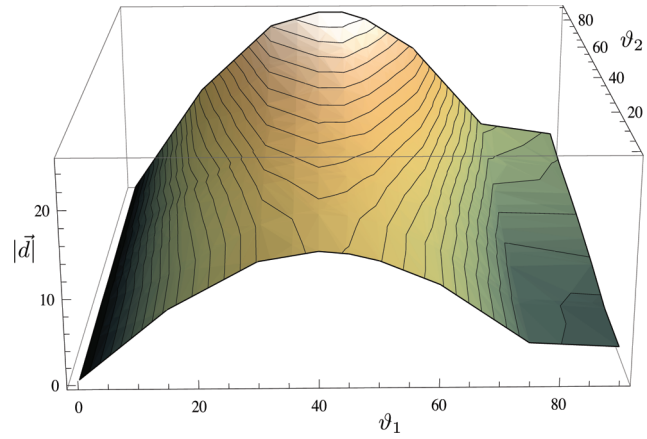

Figure 2. Norm of the DM vector (in cm^{-1}) as function of the ϑ_1 and ϑ_2 deformation angles (in deg) obtained at the CAS(2/2)/RASSI-SO level.

The observed behavior is apparently not due to one single, simple mechanism but to the sum of several, complementary or opposing, mechanisms. In the next section, we will describe the origin of the dominant mechanisms that lead to DM interaction and relate the findings to the shape of the surface shown in Figure 2.

3.4. Description of the Dominant Mechanisms. The results described in the previous section strongly suggest that the dominant mechanisms leading to DM interactions occur at the first order of perturbation, that is, a direct coupling between the magnetic singlet and triplet spin-free states via spin−orbit coupling. Some of these mechanisms have been described in the literature,[17] but here we complete the analysis and classify the different mechanisms by increasing importance.

The CASSCF wave functions of the triplet and singlet state are

$$\begin{aligned} |1,1\rangle &= |\phi_s\phi_a\rangle \\ |1,0\rangle &= [|\phi_s\bar{\phi}_a\rangle - |\phi_a\bar{\phi}_s\rangle]/\sqrt{2} \\ |1,-1\rangle &= |\bar{\phi}_s\bar{\phi}_a\rangle \\ |0,0\rangle &= \lambda|\phi_s\bar{\phi}_s\rangle - \mu|\phi_a\bar{\phi}_a\rangle \end{aligned} \tag{11}$$

in which all the doubly occupied orbitals are omitted for clarity. The symmetric and antisymmetric molecular orbitals ϕ_s and ϕ_a are mainly localized on the Cu atoms but have important tails on the bridging oxygen, as shown in Figure 3. The composition of the CASSCF magnetic orbitals is as follows:

$$\begin{aligned} \phi_s &= \sum_i c_i[3d_i(l) \pm 3d_i(r)] + c_y 2p_y + \ldots \\ \phi_a &= \sum_i c'_i[3d_i(l) \mp 3d_i(r)] + c_x 2p_x + \ldots \end{aligned} \tag{12}$$

where $3d_i(l,r)$ is one of the five atomic 3d orbitals centered on the left or right Cu ion, and $2p_{x,y}$ stand for the atomic $2p_{x,y}$ orbitals on the bridging oxygen. In none of the distortions considered here does the O-$2p_z$ orbital contribute to the magnetic orbitals. In addition, all of the other contributions to the magnetic orbitals are either very small or irrelevant for the anisotropy and have been removed for

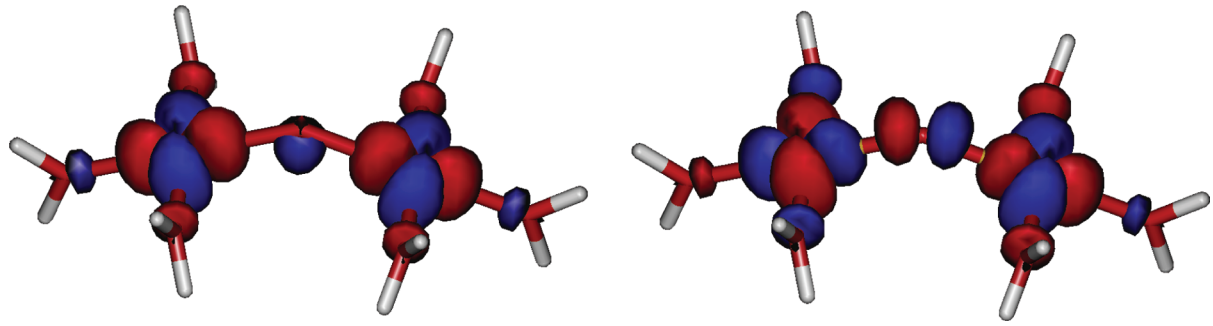

Figure 3. Symmetric (ϕ_s) and antisymmetric (ϕ_a) magnetic orbitals for the $\vartheta_1 = 40°$, $\vartheta_2 = 0°$ structure.

Table 4. List of Different Classes of Matrix Elements in the Direct Coupling after the Substitution of eqs 11 and 12 in $\langle 1,0|\hat{l}_z \cdot \hat{s}_z|0,0\rangle$[a]

class	electr. conf.	example matrix element	number
d−d (neutral)	$3d^9-2p^6-3d^9$	$\zeta_1\langle 3d_{x^2-y^2}(I)3\bar{d}_i(r)\|\hat{l}_z(I)\cdot\hat{s}_z(I)\|3d_{xy}(I)3\bar{d}_i(r)\rangle$	18/18
d−d (ionic)	$3d^8-2p^6-3d^{10}$	$\zeta_2\langle 3d_{x^2-y^2}(I)3\bar{d}_i(I)\|\hat{l}_z(I)\cdot\hat{s}_z(I)\|3d_{xy}(I)3\bar{d}_i(I)\rangle$	12/18
p−d (copper)	$3d^9-2p^5-3d^{10}$	$\zeta_1\langle 3d_{x^2-y^2}(I)2\bar{p}_j\|\hat{l}_z(I)\cdot\hat{s}_z(I)\|3d_{xy}(I)2\bar{p}_j\rangle$	24/24
p−d (oxygen)	$3d^9-2p^5-3d^{10}$	$\zeta_3\langle 3d_i(I)2\bar{p}_x\|\hat{l}_z\cdot\hat{s}_z\|3d_i(I)2\bar{p}_y\rangle$	24/24
p−p	$3d^{10}-2p^4-3d^{10}$	$\zeta_4\langle 2p_x2\bar{p}_y\|\hat{l}_z\cdot\hat{s}_z\|2p_x2\bar{p}_x\rangle$	2/2

[a] $\bar{d}_i(I)$ indicates a 3d orbital on the left Cu center occupied with a β electron. An example matrix element is given for each class together with the total number of triplet/singlet terms. ζ_1 and ζ_2 are the atomic spin−orbit parameters of Cu^{2+} and Cu^{3+}, respectively. ζ_3 and ζ_4 are the spin−orbit parameters of O^- and O, respectively.

simplicity. The resulting orbitals are renormalized before further processing.

The second and most laborious step is the substitution of eqs 11 and 12 in the expression of the coupling between singlet and triplet through the spin−orbit operator. The derivation of the complete analytical expressions for all of the points considered in the magneto-structural correlations derived in the previous section would require consideration of the four spin−orbit states and all 12 atomic orbital contributions ($2p_x$, $2p_y$, and the 10 3d orbitals) to ϕ_s and ϕ_a. This would obviously lead to an overwhelming number of terms. Therefore, it is necessary to restrict the analysis to some special points for which the dominant mechanisms can be derived, which are then extrapolated to the other cases.

The first case to be analyzed is the structure with $\vartheta_1 \neq 0$ and $\vartheta_2 = 0$. Since, the DM vector is oriented along the z axis, only the $\langle 1,0|\hat{l}_z \cdot \hat{s}_z|0,0\rangle$ coupling has to be considered. For symmetry reasons, the $3d_{xz}$ and $3d_{yz}$ atomic orbitals do not contribute to the magnetic orbitals. Moreover, the $\hat{l}_z \cdot \hat{s}_z$ operator does not couple the $3d_{z^2}$ to the $3d_{xy}$ or $3d_{x^2-y^2}$ orbital. These simplifications lead to a reasonable number of terms that can be classified in five different types. Table 4 gives an example of each class and enumerates the total number of terms in each class.

If we now focus on the structure with $\vartheta_1 = 40°$ and $\vartheta_2 = 0$, the λ and μ CI coefficients in eq 11 are 0.7275 and 0.6861, respectively.

Using the numerical expression of the optimized orbitals of the triplet (ϕ_s, ϕ_a) and singlet (ϕ'_s, ϕ'_a) orbitals given in the Supporting Information, the DM interaction can be decomposed in the five classes of interactions mentioned before. The results are collected in Table 5. In the first place, it should be noticed that the decomposition leads to a similar norm of the DM vector as the complete RASSI-SO calculation, validating the analysis. The small differences arise from the use of atomic spin−orbit parameters and the simplification of the magnetic orbitals to the essential atomic orbitals contribution.

Table 5. Contributions to the d_z Component of the DM Vector (in cm^{-1}) of the Different Types of Mechanisms at the CASSCF Level for the ($\vartheta_1 = 40°,90°;\vartheta_2 = 0°$) Structures

class	$\vartheta_1 = 40°$	$\vartheta_1 = 90°$
d−d (neutral)	13.1	0.0
d−d (ionic)	−0.2	0.0
p−d (copper)	0.1	0.0
p−d (oxygen)	0.4	1.2
p−p	−0.1	0.0
total	13.3	1.2
RASSI-SO	14.8	3.6

The largest contribution to the DM vector arises from the d−d (neutral) interactions. This term reaches a maximum when the contribution of the $3d_{x^2-y^2}$ and $3d_{xy}$ orbitals to ϕ_s and ϕ_a is largest. This happens for the structure with $\vartheta_1 = 45°$. Nevertheless, the existence of other mechanisms and the difference between λ and μ displaces the maximum to slightly smaller angles. The d−d (ionic) contribution to the DM is small in this geometry and expected to be small in all cases. The contribution of these types of interactions may increase for smaller bending angles for which the isotropic coupling is stronger, and hence, the weight of the ionic configurations is larger. However, in these cases, the contribution of the $3d_{xy}$ orbital to the magnetic orbital is reduced, leading to a counterbalancing effect.

The p−d (copper) and p−d (oxygen) contributions are negligible in this geometry due to a numerical cancellation of various contributions. This is, however, not always the case, as will become clear for the structure with $\vartheta_1 = 90°$. Finally, the contribution of the O-$2p^4$ configuration

to the wave function has such a small weight that the importance of this mechanism is negligible.

At $\vartheta_1 = 90°$, only the $3d_{xy}$ and $3d_{z^2}$ orbitals have nonzero copper contributions to the magnetic orbitals. Since these orbitals are not coupled by the $\hat{l}_z \cdot \hat{s}_z$ operator, the contributions of the d−d and p−d (copper) mechanisms are strictly zero for this geometry. The dominating effect is a p−d (oxygen) mechanism, the spin−orbit coupling on the oxygen atom in the presence of a hole on one of the copper atoms. Again, the weight of the O-$2p^4$ configuration is small, and as a consequence the contribution to the DM vector of the p−p mechanism is nearly zero.

Once we change ϑ_2 to values different from zero, the $\hat{l}^{\pm} \cdot \hat{s}^{\pm}$ operators come into play, and the coupling between all 3d atomic orbitals should be considered. This leads to a significant increase of the norm of the DM vector upon the increase of the twist angle of the two CuO_4 planes in the model complex. A numerical analysis of the mechanisms is simply too elaborate and would not really offer new insights. The main contribution to the DM interaction arises from the d−d (neutral) mechanism with smaller contributions from the other mechanisms. Close to $\vartheta_1 = 90°$, the p−d (oxygen) term dominates.

4. Conclusions

The multispin Hamiltonian of the d^9-d^9 configuration contains 10 well-defined parameters. These parameters have been extracted using the effective Hamiltonian in combination with the CASSCF/CASPT2/RASSI-SO methodology. The comparison of the numerical effective Hamiltonian with the model Hamiltonian shows that the latter one accurately describes all of the magnetic interactions contained in the exact electronic Hamiltonian.

The symmetric anisotropy terms of the multispin Hamiltonian are small. The sign of the axial anisotropy and the orientation of the magnetic axis frame cannot be determined with the applied computational strategy, it being too dependent on the details of the calculation. A more sophisticated computational scheme is compulsory to benchmark the computations for these types of interactions. However, the antisymmetric anisotropic (or DM) interactions appear more robust and can be studied with the outlined strategy. Our conclusions can be summarized in three main points.

In the first place, the DM interaction is dominated at the first order of perturbation by the direct coupling between the magnetic singlet and triplet via spin−orbit coupling. This leads to an important simplification of the computational treatment, namely, the reduction of the SI space to the magnetic states and the use of the minimal active space.

Second, the main deformations of cuprate-like materials have been studied, that is, the Cu−O−Cu bending angle and the twist angle between the copper planes. The symmetry rules for the appearance of the DM interaction and the direction of the DM vector have been verified. It is shown that the twist angle alone does not produce any significant anisotropy. However, when it is combined with the Cu−O−Cu bending, the synergic effect between both deformations can lead to a DM vector with a rather large norm.

Finally, the analysis of the leading mechanisms that contribute to the DM interactions show that the neutral d−d terms dominate and have a maximum for a bending angle close to 40°. Smaller contributions due to the spin−orbit coupling involving electrons on the oxygen bridge account for the nonzero DM interaction at 90° bending.

The approach presented here is currently being applied to *n*-center cluster of real cuprate materials in order to estimate the DM interaction and validate the model Hamilonian for $n > 2$.

Acknowledgment. Financial support has been provided by the HPC-EUROPA2 project (project number: 228398), Spanish Ministry of Science and Innovation (Project CTQ2008-06644-C02-01), the Generalitat de Catalunya (Project 2009SGR462 and *Xarxa d'R+D+I en Química Teorica i Computacional*, XRQTC) and the Agence Nationale de la Recherche (ANR) (Project TEMAMA ANR-09-BLAN-0195-01).

Supporting Information Available: Expression of the magnetic orbitals in the $\vartheta_1 = \vartheta_2 = 40°$ model structure. Values of the atomic spin−orbit constant used in the estimation of the spin−orbit coupling listed in Table 5. This material is available free of charge via the Internet at http://pubs.acs.org.

References

(1) Abragam, A.; Bleaney, B. *Electron Paramagnetic Resonance of Transition Ions*; Dover Publications: Dover, New York, 1986.

(2) Boča, R. *Theoretical Foundations of Molecular Magnetism*; Elsevier: Amsterdam, 1999.

(3) Hutchison, C. A.; Mangum, B. W. *J. Chem. Phys.* **1961**, *34*, 908–922.

(4) Kahn, O. *Molecular Magnetism*; VCH Publishers: Weinheim, Germany, 1993.

(5) Boča, R. *Coord. Chem. Rev.* **2004**, *248*, 757–815.

(6) Gatteschi, D.; Sessoli, R. *Angew. Chem., Int. Ed.* **2003**, *42*, 269–297.

(7) Thio, T.; Thurston, T. R.; Preyer, N. W.; Picone, P. J.; Kastner, M. A.; P. J. H.; Gabbe, D. R.; Chen, C. Y.; Birgeneau, R. J.; Aharony, A. *Phys. Rev. B* **1988**, *38*, 905–908.

(8) Coffey, D.; Rice, T. M.; Zhang, F. C. *Phys. Rev. B* **1991**, *44*, 10112–10116.

(9) Dzyaloshinskii, I. *J. Phys. Chem. Solids* **1958**, *4*, 241–255.

(10) Moriya, T. *Phys. Rev.* **1960**, *120*, 91–98.

(11) Zorko, A.; Arčon, D.; van Tol, H.; Brunel, L.-C. *Phys. Rev. B* **2004**, *69*, 174420.

(12) Zorko, A.; Nellutla, S.; van Tol, J.; Brunel, L.-C.; Bert, F.; Duc, F.; Trombe, J.-C.; de Vries, M. A.; Harrison, A.; Mendels, P. *Phys. Rev. Lett.* **2008**, *101*, 026405.

(13) Yildirim, T.; Harris, A. B.; Entin-Wohlman, O.; Aharony, A. *Phys. Rev. Lett.* **1994**, *73*, 2919–2922.

(14) Koshibae, W.; Ohta, Y.; Maekawa, S. *Phys. Rev. B* **1994**, *50*, 3767–3778.

(15) Entin-Wohlman, O.; Harris, A. B.; Aharony, A. *Phys. Rev. B* **1996**, *53*, 11661–11670.

(16) Yushankai, V. Y.; Hayn, R. *Europhys. Lett.* **1999**, *47*, 116–121.

(17) Moskvin, A. S. *J. Exp. Theor. Phys.* **2007**, *104*, 913–927.

(18) Webb, S. P.; Gordon, M. S. *J. Chem. Phys.* **1998**, *109*, 919–927.

(19) Pederson, M. R.; Jackson, K. A. *Phys. Rev. B* **1990**, *41*, 7453–7461.

(20) Jackson, K. A.; Pederson, M. R. *Phys. Rev. B* **1990**, *42*, 3276–3281.

(21) Pederson, M. R.; Khanna, S. N. *Phys. Rev. B* **1999**, *60*, 9566–9572.

(22) Baruah, T.; Pederson, M. R. *Int. J. Quantum Chem.* **2003**, *93*, 324–331.

(23) Kortus, J.; Pederson, M. R.; Baruah, T.; Bernstein, N.; Hellberg, C. S. *Polyhedron* **2003**, *22*, 1871–1876.

(24) Park, K.; Pederson, M. R.; Richardson, S. L.; Aliaga-Alcalde, N.; Christou, G. *Phys. Rev. B* **2003**, *68*, 020405.

(25) Ribas-Ariño, J.; Baruah, T.; Pederson, M. R. *J. Chem. Phys.* **2005**, *123*, 044303.

(26) Ribas-Ariño, J.; Baruah, T.; Pederson, M. R. *J. Am. Chem. Soc.* **2006**, *128*, 9497–9505.

(27) Ruiz, E.; Cirera, J.; Cano, J.; Alvarez, S.; Loose, C.; Kortus, J. *Chem. Commun.* **2008**, 52–54.

(28) Vahtras, O.; Loboda, O.; Minaev, B.; Ågren, H.; Ruud, K. *Chem. Phys.* **2002**, *279*, 133–142.

(29) Neese, F. *ORCA*, version 2.6; University of Bonn: Bonn, Germany, 2008.

(30) Ganyushin, D.; Neese, F. *J. Chem. Phys.* **2006**, *125*, 024103.

(31) Neese, F. *J. Am. Chem. Soc.* **2006**, *128*, 10213–10222.

(32) Neese, F. *J. Chem. Phys.* **2007**, *127*, 164112.

(33) Sinnecker, S.; Neese, F. *J. Phys. Chem. A* **2006**, *110*, 12267–12275.

(34) Duboc, C.; Phoeung, T.; Zein, S.; Pécaut, J.; Collomb, M.-N.; Neese, F. *Inorg. Chem.* **2007**, *46*, 4905–4916.

(35) Ganyushin, D.; Neese, F. *J. Chem. Phys.* **2008**, *128*, 114117.

(36) Zein, S.; Duboc, C.; Lubitz, W.; Neese, F. *Inorg. Chem.* **2008**, *47*, 134–142.

(37) Zein, S.; Neese, F. *J. Phys. Chem. A* **2008**, *112*, 7976–7983.

(38) Liakos, D. G.; Ganyushin, D.; Neese, F. *Inorg. Chem.* **2009**, *48*, 10572–10580.

(39) Karlström, G.; Lindh, R.; Malmqvist, P.-Å.; Roos, B. O.; Ryde, U.; Veryazov, V.; Widmark, P.-O.; Cossi, M.; Schimmelpfennig, B.; Neogrady, P.; Seijo, L. *Comput. Mater. Sci.* **2003**, *28*, 222–239.

(40) Malmqvist, P.-Å.; Roos, B. O.; Schimmelpfennig, B. *Chem. Phys. Lett.* **2002**, *357*, 230–240.

(41) Roos, B. O.; Malmqvist, P.-Å. *Phys. Chem. Chem. Phys.* **2004**, *6*, 2919–2927.

(42) de Graaf, C.; Sousa, C. *Int. J. Quantum Chem.* **2006**, *106*, 2470–2478.

(43) Petit, S.; Pilet, G.; Luneau, D.; Chibotaru, L.; Ungur, L. *Dalton Trans.* **2007**, 4582–4588.

(44) Chibotaru, L.; Ungur, L.; Aronica, C.; Elmoll, H.; Pilet, G.; Luneau, D. *J. Am. Chem. Soc.* **2008**, *130*, 12445–12455.

(45) Chibotaru, L.; Ungur, L.; Soncini, A. *Angew. Chem., Int. Ed.* **2008**, *47*, 4126–4129.

(46) Soncini, A.; Chibotaru, L. *Phys. Rev. B* **2008**, *77*, 220406.

(47) Maurice, R.; Bastardis, R.; de Graaf, C.; Suaud, N.; Mallah, T.; Guihery, N. *J. Chem. Theory Comput.* **2009**, *5*, 2977–2984.

(48) Maurice, R.; Guihé ry, N.; Bastardis, R.; de Graaf, C. *J. Chem. Theory Comput.* **2010**, *6*, 55–65.

(49) Maurice, R.; de Graaf, C.; Guihéry, N. *Phys. Rev. B* **2010**, *81*, 214427.

(50) Gilka, N.; Taylor, P. R.; Marian, C. M. *J. Chem. Phys.* **2008**, *129*, 044102.

(51) Sugisaki, K.; Toyota, K.; Sato, K.; Shiomi, D.; Kitagawa, M.; Takui, T. *Chem. Phys. Lett.* **2009**, *477*, 369–373.

(52) Bleaney, B.; Bowers, K. D. *Proc. R. Soc. London, Ser. A* **1952**, *214*, 451–465.

(53) Gregson, A. K.; Martin, R. L.; Mitra, S. *Proc. R. Soc. London, Ser. A* **1971**, *320*, 473–486.

(54) Ross, P. K.; Allendorf, M. D.; Solomon, E. I. *J. Am. Chem. Soc.* **1989**, *111*, 4009–4021.

(55) Ozarowski, A. *Inorg. Chem.* **2008**, *47*, 9760–9762.

(56) Bencini, A.; Gatteschi, D. *Mol. Phys.* **1982**, *47*, 161–169.

(57) Kahn, O. *Angew. Chem., Int. Ed.* **1985**, *24*, 834–850.

(58) Kauffmann, K. E.; Popescu, C. V.; Dong, Y.; Lipscomb, J. D.; Que, L., Jr.; Münck, E. *J. Am. Chem. Soc.* **1998**, *120*, 8739–8746.

(59) Yoon, J.; Mirica, L. M.; Stack, D. P.; Solomon, E. I. *J. Am. Chem. Soc.* **2004**, *126*, 12586–12595.

(60) Bloch, C. *Nucl. Phys.* **1958**, *6*, 329–347.

(61) des Cloizeaux, J. *Nucl. Phys.* **1960**, *20*, 321–346.

(62) Buckingham, A. D.; Pyykko, P.; Robert, J. B.; Wiesenfeld, L. *Mol. Phys.* **1982**, *46*, 177–182.

(63) Harriman, J. E. *Theoretical Foundations of Electron Spin Resonance*; Academic Press: New York, 1978.

(64) Douglas, N.; Kroll, N. M. *Ann. Phys. (Leipzig)* **1974**, *82*, 89.

(65) Hess, B. A. *Phys. Rev. A* **1986**, *33*, 3742–3748.

(66) Hess, B. A.; Marian, C. M.; Wahlgren, U.; Gropen, O. *Chem. Phys. Lett.* **1996**, *251*, 365–371.

(67) Schimmelpfenning, B. *AMFI*; Stockholms Universitet: Stockholm, Sweden, 1996.

(68) Christiansen, O.; Gauss, J.; Schimmelpfenning, B. *Phys. Chem. Chem. Phys.* **2000**, *2*, 965–971.

(69) Llusar, R.; Casarrubios, M.; Barandiarán, Z.; Seijo, L. *J. Chem. Phys.* **1996**, *105*, 5321–5330.

(70) Barandiaran, Z.; Seijo, L. *J. Chem. Phys.* **2003**, *118*, 7439–7456.

(71) Queralt, N.; Taratiel, D.; de Graaf, C.; Caballol, R.; Cimiraglia, R.; Angeli, C. *J. Comput. Chem.* **2008**, *29*, 994–1003.

(72) Andersson, K.; Malmqvist, P.-Å.; Roos, B. O. *J. Chem. Phys.* **1992**, *96*, 1218–1226.

(73) Ghigo, G.; Roos, B. O.; Malmqvist, P.-Å. *Chem. Phys. Lett.* **2004**, *396*, 142–149.

(74) Forsberg, N.; Malmqvist, P.-Å. *Chem. Phys. Lett.* **1997**, *274*, 196–204.

(75) Roos, B. O.; Lindh, R.; Malmqvist, P.-Å.; Veryazov, V.; Widmark, P.-O. *J. Phys. Chem. A* **2005**, *109*, 6575−6579.

(76) Van den Heuvel, W.; Chibotaru, L. *Inorg. Chem.* **2009**, *48*, 7557–7563.

(77) Anderson, P. W. *Phys. Rev.* **1950**, *79*, 350–356.

(78) Goodenough, J. B. *Phys. Rev.* **1955**, *100*, 564–573.

(79) Kanamori, J. *J. Phys. Chem. Solids* **1959**, *10*, 87–98.

CT100329N